Effects of CO_2-absorption control strategies on the dynamic performance of a supercritical pulverized-coal-fired power plant

Stefanía Ó. Garðarsdóttir[a], Rubén M. Montañés[b], Fredrik Normann[a], Lars O. Nord[b], Filip Johnsson[a]

a Department of Energy and Environment, Chalmers University of Technology, S-412 96 Göteborg, Sweden

b Department of Energy and Process Engineering, NTNU - Norwegian University of Science and Technology, Trondheim, Norway

Abstract

This work investigates the interactions that occur between a supercritical pulverized-coal-fired power plant and a downstream CO_2-absorption process during load changes in the power plant, by linking the dynamic models of the two systems. The derived dynamic model for this integrated system is implemented in the dynamic modeling and simulation software Dymola. The operation of the integrated system is investigated in two modes of operation, considering various power plant loads and levels of steam availability for the CO_2-absorption process. Several schemes for control of the CO_2-absorption process, which have been suggested in the literature, are implemented for the integrated system and their effects on power plant operation are evaluated.

Comparison of the simulation results obtained through varying the power plant load with and without CO_2 absorption reveal that the CO_2-absorption process has slower process dynamics than the power plant cycle, with the CO_2 absorption stabilizing in more than 1 hour, while the power generation generally stabilizes in 6–9 minutes, in the power plant both with and without CO_2 absorption. The control scheme used for the CO_2-absorption process is important, as pairing of the control variables in relatively slow control loops increases the settling time of the power plant by up to 30 minutes with respect to power output. The results suggest that the investigated CO_2-absorption process does not affect significantly the load-following capabilities of the power plant. Redirecting steam from the CO_2-absorption process to the low-pressure turbine section in order to increase power generation (during a hypothetical peak-load demand) results in fluctuations of process variables in the power plant during the 2 hours of reduced steam availability to the CO_2-absorption process. This is observed for both control schemes applied to the CO_2-absorption process, and the power generation is not stabilized until the operation is restored to full load.

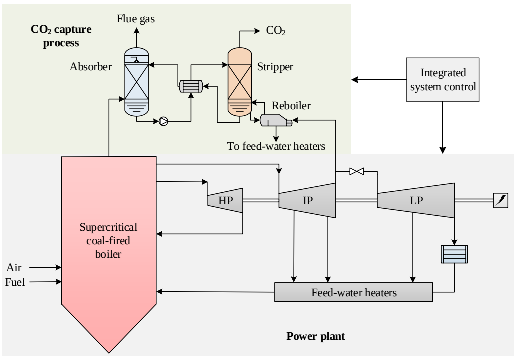

1 Introduction

The increasing capacity of variable renewable electricity (VRE) in today´s energy system is promoted by energy policies that are aimed at reducing carbon dioxide (CO_2) emissions from the power generation sector and at reducing the dependency on fossil fuels for thermal power generation [1]. Due to the relatively low operating costs of VRE, i.e., mainly wind and solar, such production units are positioned early in the dispatch order, when they are available [2]. Thus, the increased VRE capacity in the electricity production mix is decreasing demand for base-load power generation and increasing demand for regulating power. The conventional generating units (which are based on fossil fuel combustion) that remain in the production mix will therefore have to assume a new role in providing flexibility management where part-load characteristics are of increasing importance. Existing and future thermal power generation units also face increased pressure to decrease their CO_2 emissions. Carbon capture and storage technologies are essentially the only option available for fossil-based power generation in a future CO_2-constrained world, and if these plants will be required to operate in a flexible manner, the requirement must also include the CO_2-capture process.

Post-combustion CO_2 capture based on chemical absorption with amines, which is widely regarded as a state-of-the-art technology for CO_2 capture [3], is currently operating on a commercial scale [4]. Thus, the capture process will inevitably affect power plant performance on steady-state and dynamic bases, since the CO_2-capture process requires for its operation energy in the form of steam from the power plant. Therefore, the CO_2-capture process has to be operated in a way that minimizes disturbances in the of power generation.

Efforts to evaluate the dynamic performance of absorption-based CO_2 capture have increased considerably over the last decade, as discussed in the recent review by Bui, et al. [5]. In the majority of the studies published to date on this subject, the focus has been primarily on the dynamic behavior and controllability of the CO_2-capture process and less so on the connection to and influence on the power plant controllability and process dynamics. Studies that have developed schemes for controlling CO_2 absorption [e.g., [6-11]] generally identify the same degrees of freedom (DoFs) in the absorption process. The DoFs represent the number of variables that have to be set to define fully the state of the process. After satisfying the requirements for regulatory control and process equality constraints, i.e., the control of liquid levels, the control of cooling water flow for the solvent cooler and CO_2 product condenser, as well as the control of stripper pressure using the CO_2 product valve, the remaining variables to manipulate (MVs) are the solvent circulation rate ($\dot{m}_s$) and the flow rate of steam to the reboiler ($\dot{m}_{steam}$). These two MVs are paired with higher-level control variables (CVs), i.e., variables that define the CO_2-capture process performance with respect to energy demand and CO_2 removal requirements. These are most often the CO_2-capture rate and a specific temperature somewhere in the process, e.g., the reboiler temperature.

Ziaii [6] developed a dynamic model of an MEA-based absorption process and evaluated several control schemes for a system that involved part-load operation of the power plant and a reduction in reboiler load. A steady-state model of the turbine section of a coal power plant was used to determine the off-design steam conditions. Ziaii concluded that an advanced multi-variable control scheme may not be necessary for the CO_2-absorption process. Instead, they proposed a strategy whereby the solvent circulation rate is controlled to achieve a specific target for different load conditions, rather than to control the CO_2 removal rate explicitly. The similar performance of MPC controllers and more simple decentralized controllers was further confirmed by Cormos, et al. [7]. Panahi and Skogestad [8] and [9] developed several control schemes for a CO_2-capture process in which MEA was used with simple absorber-stripper setup. In these studies, it was also concluded that a simple decentralized control scheme was the most feasible, as this scheme showed performance similar to that of a more complex model predictive control (MPC) scheme and was easier to implement. In the proposed scheme, the mass flow of steam ($\dot{m}_{steam}$) is used to control the CO_2 removal rate, and the solvent circulation rate downstream of the absorber is manipulated to maintain a set temperature at a specific stage in the stripper. The same control scheme was presented by Gaspar, et al. [10] based on a Relative Gain Array analysis, though a subsequent sensitivity analysis suggested opposite pairing of control and manipulated variables. Nittaya, et al. [11] have presented a controllability study of an MEA-based absorption unit, in which they have developed three decentralized control schemes for an MEA-based absorption process with a simple absorber-stripper setup and evaluated the performances of the schemes in several scenarios, including a change in the flue gas flow rate, a change in the CO_2-capture rate, and a valve stiction. The studies conducted by [7-11] do not include a model of a power plant. Walters, et al. [12] used a low-order model of a piperazine (PZ)-based CO_2-absorption plant conditions to develop control schemes for different system objectives, including the control of CO_2 delivery to an enhanced oil recovery (EOR) facility and peak electricity production. The boundary conditions were created using a steady-state model of a supercritical power plant. They concluded that when the focus is on fulfilling the requirements of one of the systems, i.e., the power plant, CO_2-absorption plant or the EOR facility, the dynamic performances of the other systems suffer.

Several studies have in addition considered the power plant operation, albeit to different extents. Most notable in this context is the study performed by Lawal, et al. [13], which included a dynamic model of a sub-critical, coal-fired plant. That study concluded that the CO_2-absorption process has a slower response to load changes than the power plant, and that control loops in the capture process may interfere with power plant control loops, resulting in unsteady power output. More recently, Wellner, et al. [14] developed an integrated dynamic model of a supercritical, coal-fired plant with CO_2-absorption. They concluded that reliable primary frequency control could be provided by the integrated system by redirecting steam from the CO_2-absorption process to the power plant. In the studies conducted by Mac Dowell and Shah [15, 16], a simple model of a sub-critical power plant was developed, in order to specify the flue gas flow and composition, as well as the state of the steam supplied to the CO_2-capture process. In those studies, the focus was on evaluating and optimizing the base-load and part-load operating modes of the integrated system from a techno-economic perspective, where they concluded that operating with either a time-varying solvent regeneration or a solvent storage system could increase profitability, as compared to operating with a relatively constant CO_2-capture rate under load-following conditions. However, the power plant dynamics were not considered in that model. Hanak, et al. [17] studied the off-design performance of an integrated supercritical coal-fired power plant with monoethanolamine (MEA)-based CO_2 capture under steady-state conditions. They, as well as Garðarsdóttir, et al. [18], have highlighted the importance of taking into account off-design conditions in the steam cycle, i.e., the drop in pressure in the low-pressure section of the turbine due to steam being extracted to the CO_2-capture process, to avoid over-estimating the thermal efficiency of the system under part-load conditions.

In summary, the literature proposes a series of control schemes for the CO_2-absorption process for operating the system under various process conditions. However, the majority of the previous studies carried out on CO_2-absorption process dynamics have assumed perfect boundary conditions, in terms of flue gas flow and steam supply to the process, thereby disregarding the potential interactions of the two non-linear feedback systems, i.e., the CO_2-absorption process and the power plant. Therefore, it remains unclear as to how the integrated system behaves and should be controlled. In order to propose control schemes, there is a need for improved understanding of the interactions that occur between the power plant and the capture process.

This study investigates the dynamic operation of an integrated CO_2 absorption–thermal power plant. The aim was to investigate how the control strategies proposed for the MEA-based CO_2-absorption process perform when taking into account integration with a power plant. The framework considered for operation of the power plant is a day-ahead energy market with an hourly production scheduled; thus, there is no consideration of the fast response required for frequency control services [19]. Two modes of transient operation, varying the power plant load and varying the steam availability for CO_2 capture, are investigated, to consider different operational objectives for the CO_2-capture plant. The studied power plant is a supercritical pulverized fuel (PF) coal-fired plant. The dynamic model of the integrated system is based on the multi-domain, open modeling language Modelica [20], and is developed in the Modelica-based, commercial Dymola software.

2 Methodology

Figure 1 gives an overview of the cases investigated in this work. The dynamic operation of the integrated system was studied under two modes of operation: varying the power plant load; and varying the availability of steam for the CO_2-absorption process, together yielding three different operational cases to which several control schemes for the CO_2-absorption process were tested. The modes of operation and the different control schemes are described in detail in Section 5.1. The performance of the integrated system was evaluated with respect to key performance indicators, such as power plant efficiency and the specific energy requirements of the CO_2-absorption process on both steady-state and dynamic bases, including analyses of the response times and settling times (95% and 99%) for the selected performance indicators. The settling time is the time that it takes for the system output to reach and stay within ±5% and 1%, respectively, of the final steady-state output value compared to the steady-state output value before a disturbance is introduced into the system. It should be noted that in an ideal situation, the settling time is assessed against a step-change disturbance. In the present study, disturbances are introduced to the system through ramps, so as to be more representative of reality.

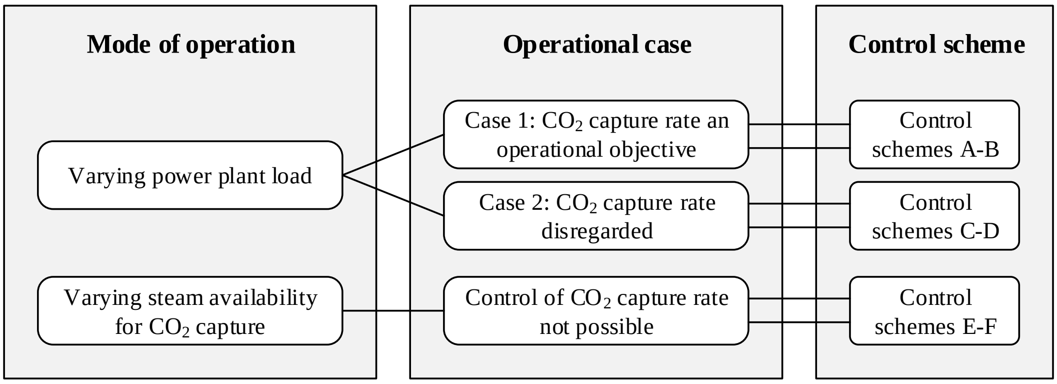

Figure 1: Investigated modes of operation, subsequent operational cases and control schemes.

The dynamic model consists of two parts, the power plant (boiler, steam cycle, and flue gas path) and the absorption plant. The power plant model represents a simplified version of a detailed steady-state model of the reference plant (Nordjyllandsvaerket in Denmark [21]). The power plant model includes all the key features of a modern power plant, such as sliding-pressure operation, steam reheating, multi-stage turbines, and open and closed feed-water heating, and should therefore represent its dynamic characteristics. The simplified version of the model is initially constructed at steady-state in the commercial power plant design software Ebsilon Professional to provide plant performance design data under full and part-load conditions. The dynamic power plant model, constructed in Dymola, mainly comprises components from Modelon´s Thermal Power Library [22]. Design data from the reference power plant [21] are used to dimension several of the modeled components. The CO_2-absorption process considered is a standard MEA cycle. The dynamic CO_2-absorption process model is based on a detailed reaction model that has been constructed in the steady-state simulation software Aspen Plus and subsequently implemented in the dynamic modeling environment of Dymola. The dynamic model of the CO_2-absorption process consists of components from Modelon´s Gas-Liquid Contactors Library [23].

Two of the key performance indicators used in the present work are the power plant electric efficiency, η_{el}, and the CO_2-capture rate, η_{CO2}, as defined by Eqs. (1) and (2):

$$\eta_{el} = \frac{P_{el}-P_{aux}}{\dot{m}_{fuel}LHV} \quad (1)$$

where P_{el} is the generated power output, P_{aux} is the power required to drive the power plant´s air compressor, flue gas fan and pumps in the steam cycle, $\dot{m}_{fuel}$ is the mass flow of fuel and LHV is the lower heating value of the fuel. This definition is used for the power plant with and without CO_2 absorption and does not consider the electricity needed for the CO_2-absorption process.

$$\eta_{CO2} = \frac{\dot{m}_{CO2,in} - \dot{m}_{CO2,out}}{\dot{m}_{CO2,in}} \quad (2)$$

where $\dot{m}_{CO2,in}$ and $\dot{m}_{CO2,out}$ are the mass flows of CO_2 at the flue gas inlet and outlet of the CO_2 absorber, respectively.

3 Power plant modeling

The modeled power plant is a supercritical, single-reheat, PF-fired plant and is a typical representation of a modern power plant and its dynamic characteristics. The power plant model incorporates the main aspects of state-of-the-art PF power plants operated in Europe, such as sliding-pressure operation, steam reheating, multiple-stage turbines, and a feed-water heating (FWH) system and an outlet temperature control for live and reheat steam. Furthermore, a main feature of these state-of-the-art PF power plants is high electrical efficiency, generally in the range of 42%–47%, when operated under design conditions. A schematic overview of the dynamic power plant model including flow controllers and measurement points is presented in the Supplementary material, Figure S1. The power plant has a design capacity of 408 MW_{el} with electric efficiency of 45.1% as defined in Equation 1. The power plant operates on a pulverized bituminous coal with the composition listed in Table 1, a higher heating value (HHV) of 26.91 MJ/kg, and a lower heating value (LHV) of 25.18 MJ/kg. Below is a description of the main modeling assumptions made to describe the dynamic power plant boiler, steam cycle, flue gas pathway, and control scheme.

Table 1: Fuel specification in the power plant model[21].

Component	Composition, as received [wt%]
C	63.0
H	4.3
N	1.4
S	0.8
O	7.5
Moisture	14.0
Ash	9.0

Supercritical boiler

The boiler model includes a furnace, to which a fuel boundary condition is connected, and a description of the heat transfer between the gas and the water side. The heat transfer is described by six heat-exchanging sections, i.e., water wall, two stages of superheating, two stages of reheating, and an economizer (in the order of the gas flow). If necessary, a water spray is used to control the steam temperature at the inlet of the HP and IP turbines, by injecting HP feed-water between the two stages of the superheater (SH1 and SH2) and the reheater (RH1 and RH2).

Furnace section

The furnace model is zero-dimensional, being described by a static energy balance, and assumes complete combustion. The steady-state energy balance of the furnace is defined as:

$$\dot{m}_{air,in} h_{air,in} + \dot{m}_{fuel} HHV = \dot{m}_{gas,out} h_{gas,out} \quad (3)$$

where the enthalpies of the air, $h_{air,in}$, and flue gas, $h_{gas,out}$, are calculated as a function of the stream temperature, composition and pressure.

<u>Superheating sections, water walls and economizer</u>

The gas-water heat-exchanging sections are modeled as discretized pipe models with lumped pressure on both sides and with a discretized dynamic wall model connecting the two pipes. Dynamic equations are used to describe the water-side mass and energy balances. The gas volume dynamics are assumed to be rapid and are described as steady-state in the superheater, reheater, and economizer components. However, a separate realistic gas volume (based on plant data from Nordjyllandsvaerket) is included together with the heat exchangers, to account for the residence times. A similar approach is used for the water walls. The gas side of the water walls is described as a single volume (without pressure drop) to consider the residence time, and a flow resistance component is used to account for the pressure drop. A wall component describes the heat transfer through the wall and a dynamic pipe component describes the water-side dynamics. The general dynamics equations for energy and mass on the water side are expressed in Eqs. (4) and (5), respectively:

$$V\rho\frac{dh}{dt} = \dot{m}_{in}h_{in} - \dot{m}_{out}h_{out} + V\frac{dp}{dt} + Q \quad (4)$$

$$\frac{dm}{dt} = V\left(\frac{d\rho}{dh}\frac{dh}{dt} + \frac{d\rho}{dp}\frac{dp}{dt}\right) \quad (5)$$

where V and ρ are the fluid volume and density, and h_{in}, h_{out} and $\dot{m}_{in}$, $\dot{m}_{out}$ are the inlet and outlet enthalpies and mass flows of the fluid, respectively. With p as the pipe pressure, the heat transferred through the pipe wall, Q, is determined from:

$$Q = \alpha A_{heat}\left(T_{wall} - T_{fluid}\right) \quad (6)$$

The heat transfer area, A_{heat}, in the boiler heat-exchanging sections is approximated from Nordjyllandsvaerket plant data. The heat transfer coefficient, α, on the water side is set at a constant of 1500 W/m^2*K in all the sections, in accordance with previous work [24]. The gas-side heat-transfer coefficient, which is the limiting factor for heat transfer, is estimated from Nordjyllandsvaerket plant data under design conditions for the different heat-transfer sections. The heat transfer coefficient at off-design conditions (U) is calculated from the mass flow (m_0) and the heat transfer coefficient (U_0) under design conditions, and the off-design mass flow (m) is calculated according to Eq. (7) [25-26]. The exponent, *n*, depends on the geometry of the heat exchanger and is estimated from plant data (for the derived values in each boiler section, see the Table S1, Supplementary material). This approach is therefore not dependent upon the geometry of the heat-exchanging sections, but rather on the total heat exchanger area of each section. Note that the same approach is applied to the water wall section, and that the model does not distinguish between convective and radiative heat transfer, as they are lumped together in the empirical heat transfer coefficient expression, which is applied as:

$$U = U_0\left(\frac{m}{m_0}\right)^n \quad (7)$$

Steam cycle

The steam cycle includes three turbine sections (HP, IP and LP), with a reheat between the first and the second section, and the IP and LP sections comprising two turbine stages each. The feed-water system consists of a steam turbine condenser connected to a cooling water boundary condition, two closed feed-water heaters, one open feed-water heater (a deaerator), as well as three feed-water pumps.

The turbine stages are modeled in steady state, with Stodola´s law being used for determining the off-design performance of the turbines [27]. A isentropic efficiency of 0.88 was used [28], and a Baumann coefficient of 0.3 was used for the last turbine stage to account for the decrease in efficiency attributed to the moisture content of the steam [29]. The thermodynamic properties of the turbine shaft are not taken into consideration, i.e., temperatures in the shaft are not modeled other than the temperatures at the inlet and outlet of each turbine stage. The thermal mass and the inertia of the shaft are not accounted for. This simplified modeling approach for the steam turbine is justified by the turbine inertia being of relatively low importance compared with other parts of the system, i.e., the boiler and feed-water heating system, for the time-scales considered in this work [30].

The steam turbine condenser and closed feed-water heaters are modeled as cylindrical vessels, with thermodynamic equilibrium between the liquid and vapor phases. Thus, sub-cooling of the condensate is not considered. The condensate level is monitored and assertion is given if the volume is emptied or filled up with liquid, which stops the simulation. The heat transfer area is assumed to be independent of the liquid level. The pressure loss on the cooling side is assumed to be negligible. The residence time in the steam turbine condensers' and the closed feed-water heaters' hotwell is assumed to be 2 minutes under design conditions [31]. The dynamic mass and energy balances of the steam turbine condenser and closed feed-water heaters are expressed by Eqs. (8) and (9), respectively:

$$\frac{dM}{dt} = \dot{m}_{in} - \dot{m}_{out} \tag{8}$$

$$\frac{dE}{dt} = \dot{m}_{in}h_{in} - \dot{m}_{out}h_{out} + Q \tag{9}$$

where Q is the heat transferred through the tube bundles, calculated with Eq. (6) using a heat transfer correlation for condensation over the tube bundles [32] on the steam side. On the cold side, a heat transfer correlation for one-phase pipe flow, applicable to both laminar and turbulent flow, is used [33].

The deaerator is modeled as a cylindrical vessel with thermodynamic equilibrium between the liquid and vapor phases. The dynamics of the metal wall are described as the heat transfer between the metal wall and the two-phase fluid, as well as the external atmosphere. The metal wall is assumed to have a uniform temperature. The chemical processes that are involved in the deaeration process, to remove dissolved gases, are not considered in the model. The design criterion for the deaerator volume is a residence time of 2 minutes [31]. The power plant is assumed to have access to cooling water at a temperature of 15°C, and no further constraints or dynamics with respect to the cooling water source are taken into account. Feed-water pumps are modeled as centrifugal pumps with quadratic characteristics. All valves in the steam cycle are assumed to have linear characteristics, with the ratio of mass flow to pressure drop under design conditions being used to calculate the pressure drop under off-design conditions. The generator is described as operating at a fixed frequency of 50 Hz[34] and a constant efficiency of 0.986 [21].

Flue gas train

The model of the flue gas train includes an electrically driven air compressor, an air preheater, a flue gas fan, and a cooling condenser prior to the CO_2-absorption process. Other types of flue gas-cleaning equipment, e.g., particle separation and wet flue gas desulfurization with limestone scrubbing, are not modeled in detail but are represented by a pressure drop, a volume (residence time), and a component that filters out all the gas components, with the exceptions of N_2, O_2, CO_2 and H_2O.

The compressor is modeled as a polytropic process along the flow path, whereby mechanical power is transferred through the component *via* a rotational mechanical axis. The model, which assumes that there is no internal mass flow leakage, is computed with static mass and energy balances. The isentropic and mechanical efficiencies are set at 0.85 and 0.97, respectively [21]. A control signal to the compressor determines the mass flow through the compressor. The flue gas-cleaning equipment is represented as a flow resistance model, resulting in a specific pressure drop, and a gas volume model, which yields a specific residence time. The removal of sulfur and ash is modeled by simply setting the substance concentration to zero before the flue gases are led through the direct-contact cooler prior to the CO_2-capture process. The flue gas fan is modeled as an axial fan with constant speed.

Power plant control system

The control system of a power plant can be divided into two hierarchical layers. The top layer is the load set-point. A pre-determined load (in terms of generator output) gives an input to the boiler master controller, which in turn controls the fuel firing rate, as well as the flows of air and feed-water in the system. The flows of air and feed-water are controlled according to a predetermined ratio to the fuel flow, which depends on the load, and are derived under steady-state design conditions. The second level is the regulatory control layer, which includes temperature control of the live and reheat steam with water attemperation, i.e., evaporative spray cooling between the primary and secondary superheater and reheater stages. The regulatory control layer also includes control of the water levels in all but one of the feed-water heaters. The water level in the deaerator is allowed to fluctuate freely, for inventory consistency [35]. The pump speeds of the LP pump (downstream of the condenser) and the IP pump (downstream of the LP preheater) are used to regulate the water level in the condenser and the LP preheater, respectively. The water level in the HP preheater is regulated *via* a control valve that is located between the HP condensate outlet and the inlet of the deaerator. The PI controllers in the power plant model were initially tuned with an open loop approach and retuned in the closed loop system to further improve system response; the resulting tuning parameters are listed in Table S2, Supplementary Material.

4 CO_2-absorption process modeling

Figure 2 presents a schematic of the modeled MEA-based CO_2-capture process, including the measurement points for the control variables and flow manipulators, indicating the system DoFs. The identified DoFs in the system are the five flow manipulators (pumps and valves), designated as FC1–FC5 (Figure 2). The design parameters for the CO_2-capture process under full load conditions are presented in Table 2. Table 3 lists the residence times under the design conditions. The residence times are adapted from the work of Flø, et al. [36, 37]. The design of the CO_2-absorption process was carried out using the steady-state simulation software Aspen Plus. This includes the design of the geometry of the columns and the washing section in the absorber, the heat-exchanger area in the lean-rich heat exchanger, and the rich-loading and lean-loading of the solvent under design conditions. A detailed description of the Aspen Plus process model and the standard absorber-desorber set-up, which was used for the design, is presented elsewhere [38] with the exception that the correlations for the liquid and gas mass transfer coefficients, as well as the interface area developed by Bravo, et al. [39] are used for the process design described in the present work. In addition, Sulzer Mellapak 350Y packing is used in the present work. The dynamic model of the CO_2-absorption process has been described in detail by Garðarsdóttir, et al. [18] and Åkesson, et al. [40]. The process model has been successfully evaluated against dynamic test data for both a pilot-scale plant [40] and for a larger demonstration scale plant [41]. A significant difference between the steady-state model of the CO_2 capture process and the dynamic model constructed in Dymola is the description of the chemical reactions. In the steady-state model, reaction rates are described in terms of their kinetics, whereas in the dynamic model, chemical reactions are assumed to be at chemical equilibrium. This approach has been shown to predict dynamic responses adequately [42]. Additionally, the effect of the reaction kinetics on the gas-liquid mass transfer rates is accounted for by the use of a pseudo-first-order enhancement factor [18]. The enhancement factor is adjusted so that the performances (i.e., rich and lean solvent loadings, solvent mass flow, and the specific heat requirement in the reboiler) of the dynamic absorber and stripper columns match those of the steady-state design derived in Aspen Plus.

Several improvements have been made to the dynamic process model compared to the model presented previously [18]. The heat exchanger representation has also been improved, so that it now includes a transport delay, as identified by Flø, et al. [36]. Condensate level control is implemented on the steam side of the kettle reboiler. The reboiler volume on the solvent side and the stripper sump are aggregated with a level control in the stripper sump. A buffer tank is installed upstream of the absorber, where make-up water is injected into the system, if needed, to ensure an appropriate water balance. MEA is assumed to be non-volatile and does not exit the CO_2-absorption process with the clean flue gases or the CO_2 product, thus no MEA make-up stream is considered. This simplification is justified by the relatively short operation time considered in this work and by the low concentration of MEA derived from the process design conditions in Aspen Plus, *cf*. Table 2.

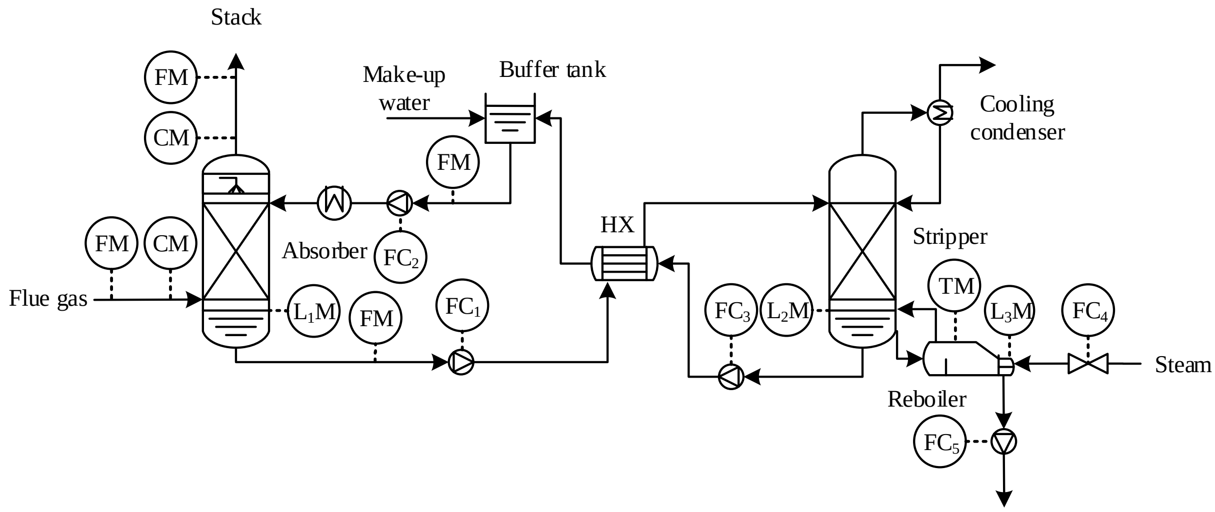

Figure 2: Schematic overview of the CO_2-absorption process model. Controllers (C) and measurement points (M) for pressure (P), flow (F), temperature (T), gas composition (C), and liquid level (L) are indicated in the figure.

Table 2: Design parameters for the CO_2 absorption process operated under full-load conditions, derived from steady-state modeling in Aspen Plus.

Absorber diameter (m)	17
Absorber packing height (m)	26
Washer section height (m)	3
Stripper diameter (m)	10.4
Stripper packing height (m)	18
Rich-lean heat exchanger area (m^2)	14,460
Rich-lean overall heat transfer coefficient (W/m^2K)	1,500
Columns' flooding limit [43]	80%
Solvent concentration (wt% MEA in CO_2-free solution)	30%
Lean loading (mol CO_2/mol MEA)*	0.28
Rich loading (mol CO_2/mol MEA)*	0.5
Direct-contact cooler discharge temperature (°C)	40
Lean cooler discharge temperature (°C)	40

CO_2 product cooling condenser temperature (°C)	20
L/G ratio (kg/kg)*	4.41
Specific reboiler duty (kJ/kg CO_2 captured)*	3,905
MEA concentration in clean flue gas (ppm)	0.3

*Values that vary according to the load.

Table 3: Solvent residence times in various pieces of the process equipment in the CO_2-absorption process under design conditions [36].

	Residence time (min)
Absorber packing	5
Absorber sump	5
Stripper packing	2
Stripper sump	10
Reboiler	5
Buffer tank	16
Lean-rich heat exchanger	26
Total system residence time	69

5 Integration with coal-fired power plant

The steam needed for solvent regeneration is extracted from the IP/LP section of the turbine. An approach of a throttled LP turbine retrofit, similar to that presented by e.g. Sanchez Fernandez, et al. [44], Liebenthal, et al. [45] and Lucquiaud and Gibbins [46] is used for the steam extraction to power the CO_2 absorption process. This approach makes the LP section of the turbine over-dimensioned for the integrated system, which operates with 90% CO_2 capture rate at full load conditions. The steam extraction line to the reboiler is throttled to maintain the extraction pressure over the whole load range, so as to maintain a suitable condensation temperature in the reboiler, thereby avoiding increased thermal degradation of the solvent. The extracted steam is de-superheated to 140°C, which is just above the saturation temperature at the extraction pressure of 3 bar, using evaporative spray cooling with the feed-water slipstream downstream of the condenser. The condensate from the reboiler is returned to the feed-water loop by pumping it into the deaerator. Figure 3 presents a schematic of the fully integrated system.

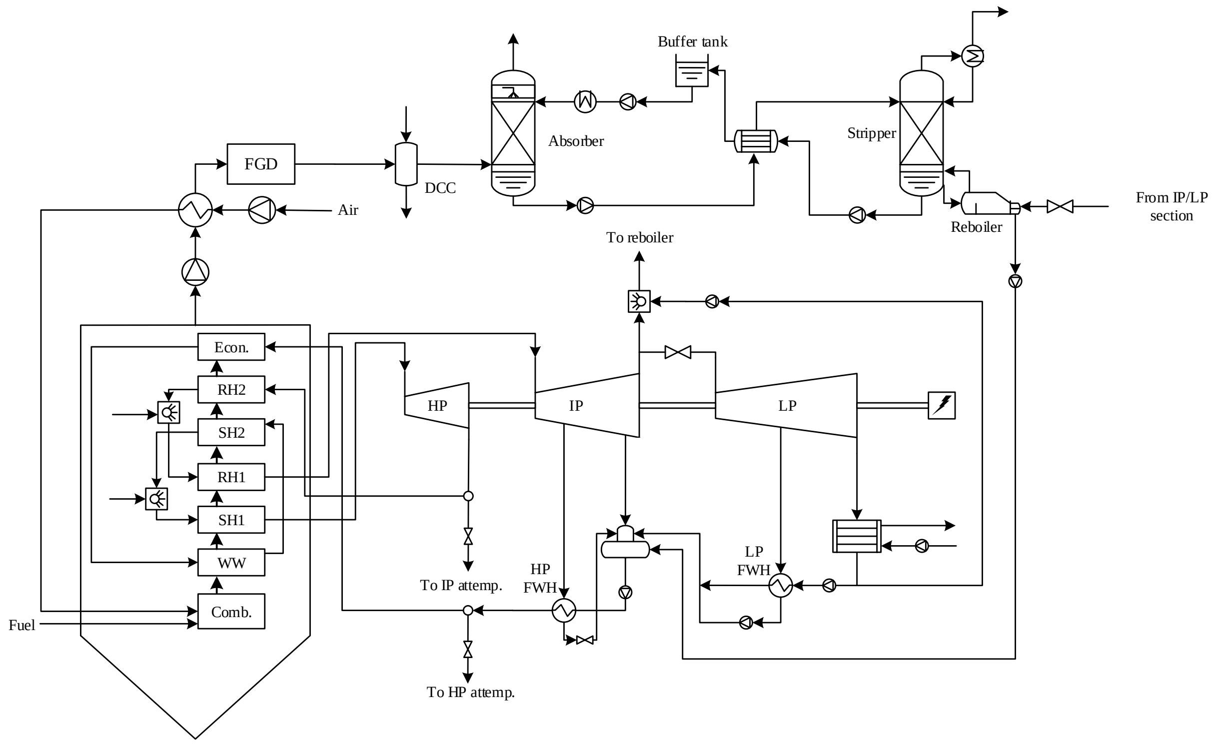

Figure 3: Process schematic showing the connections between the steam cycle and the CO_2-absorption process with a throttled LP turbine configuration for steam extraction.

5.1 Control schemes for power plant with integrated CO_2 capture

The CO_2-absorption process control system is divided into a regulatory and a higher-level control layer. The regulatory control layer is involved in the control of the liquid levels in the system, so as to achieve consistent inventory control, which is vital for process stability [35]. The available CVs in the regulatory layer are the absorber, the stripper, and the buffer tank level, as well as the make-up water stream. To ensure stable inventory control, one of the identified CVs is allowed to fluctuate freely; in this system, it is the buffer tank level. Perfect control of the make-up water stream to the buffer tank is assumed in the model, leaving two CVs in the regulatory control layers, the absorber and the stripper liquid levels, which have to be paired with one DoF each. It should also be pointed out that the condensate level of the steam side of the reboiler is regulated, as part of the regulatory control layer on the power plant side of the integrated power plant and CO_2 capture process system.

Three of the five DoFs identified in Figure 2 are, thus, designated as regulatory control variables. The higher-level control layer, which consists of the remaining two DoFs, is used to regulate those CVs identified as being important for the performance of the CO_2-absorption process. In addition, three CVs are assumed to be ideally controlled, which means that they are not included in either the regulatory or the higher-level control layer; a perfect back-pressure regulator is used to keep constant the pressure at the top of the stripper, and in both the solvent cooler and the cooling condenser, ideal temperature control is assumed. Consequently, based on the stripper outlet pressure assumption, modeling of the CO_2 compressor is omitted from this study. All of the PI controllers employed in the CO_2-capture process in the different control schemes investigated are tuned using the SIMC PID tuning rules developed by Skogestad [47].

5.1.1 Varying the power plant load: investigated control schemes

The power plant load was ramped between 90% and 70% load, as well as between 70% and 90% load at a ramp rate of 4%/min, which correspond to values commonly used in modern power plants [48]. Two cases of different operational objectives are considered with two control schemes applied in each of the two cases investigated (*cf*. Fig. 1):

Case 1: CO_2-capture rate is an operational objective

- Scheme A – The two higher-level CVs in Scheme A are the reboiler temperature and the CO_2-capture rate, which are paired with the steam flow rate (FC_4) and the solvent flow rate upstream of the absorber (FC_2), respectively. This scheme has been proposed in a series of investigations, e.g., those conducted by Jordal, et al. [49], Nittaya, et al. [11], Hanak, et al. [17] and Lawal, et al. [13], with Nittaya, et al. [11] highlighting its fast responses and ability to reject disturbances.
- Scheme B – In similarity to Scheme A, Scheme B has the higher-level objectives of controlling the reboiler temperature and CO_2-capture rate. However, the CVs are paired with the solvent flow rate downstream of the absorber (FC_1) and the steam flow rate (FC_4), respectively. Scheme B is essentially a modified version of the optimal control scheme proposed by Panahi and Skogestad [9].

Case 2: CO_2-capture rate is disregarded

- Scheme C – The two higher level CVs in Scheme C are the reboiler temperature and the L/G ratio, which are paired with the steam flow rate (FC_4) and the solvent flow rate upstream of the absorber (FC_2). Scheme C has previously been shown to decrease the heat requirement, compared with a case in which the CO_2-capture rate is a process constraint, as described by Garðarsdóttir, et al. [18].
- Scheme D – In Scheme D, only one higher-level control objective, the reboiler temperature, is considered. The CV is paired with the steam flow rate (FC_4). The solvent flow rate is dismissed as a DoF and kept constant throughout the operation. Due to its simplicity, this scheme has the potential to provide fast responses relative to Schemes A-C.

Table 4 contains all the CV-MV pairs and the resulting tuning parameters, i.e., gain (K) and time constant (τ), for all the control schemes studied with respect to operation with varying power plant load. The set-points for all the CVs are listed in Table 5 (also valid for operation with varying availability of steam for CO_2 capture).

Table 4: Tuning parameters for control schemes applied to operation with varying power plant load (Cases 1 and 2), including regulatory and higher-level controllers.

Case – Scheme	CV	MV	K	τ [s]
1 – A	L_1	FC_1	955	960
1 – A	L_2	FC_3	358	960
1 – A	L_3	FC_5	500	200
1 – A	T_{reb}	FC_4	0.11	76.7
1 – A	η_{CO2}	FC_2	2515	122
1 – B	L_1	FC_2	918	960
1 – B	L_2	FC_3	355	960
1 – B	L_3	FC_5	500	200
1 – B	T_{reb}	FC_1	157	60
1 – B	η_{CO2}	FC_4	2.94	2004.3
1 – C & D	L_1	FC_1	955	960
1 – C & D	L_2	FC_3	358	960
1 – C & D	L_3	FC_5	500	200

1 – C & D	T_{reb}	FC_4	0.11	76.7

CV, Control variable; MV, variable to manipulate; K, proportional gain; τ, time constant.

Table 5: Set-points for the CVs used in control schemes A–F.

CV	Set-point
Absorber sump level (L_1)	2.1 m
Desorber sump level (L_2)	11.5 m
Reboiler condensate level, steam side (L_3)	0.9 m
Reboiler temperature (T_{reb})	119.5 °C
CO_2 capture rate (η_{CO2})	90%
Liquid-to-gas ratio (L/G)	4.61 (kg/kg)

CV, Control variable.

5.1.2 Varying steam availability for CO_2 capture: investigated control schemes

A fraction of the steam used for solvent regeneration was re-directed to the steam cycle to increase power production. Due to that the CO_2-absorption is a retrofit to an existing boiler scheme, the LP section of the turbine becomes over-dimensioned at full load conditions in the integrated system and is therefore able to accommodate the increase in steam flow. For this type of operation, the CO_2-absorption process could be regarded as a power reserve in times of peak-load demand from the electricity system, as discussed by Chalmers, et al. [50]. The opening of the steam extraction valve between the power plant and the CO_2-absorption process was adjusted, i.e., a ramp rate of 5%/min was applied, to increase the electricity output of the power plant by 5% for 2 hours. Thereafter, the operation was returned to normal. In this mode of operation, the steam flow to the reboiler is determined by the power plant, and only one DoF remains for the capture system, i.e., the solvent flow. Consequently, there can only be one higher-level control objective. Only one operational case is considered and two control schemes, adapted from Ziaii, et al. [51], are applied:

Steam flow controlled from the power plant, control of CO_2 capture rate not possible

- Scheme E – In Scheme E, the L/G ratio in the absorber is a CV and is paired with the solvent flow rate upstream of the absorber (FC_2). As the flue gas flow to the CO_2-absorption process does not vary, the solvent flow rate is essentially kept constant resulting in a simple control scheme without higher-level feedback control loops in the CO_2 capture process.
- Scheme F – The reboiler temperature is a higher-level CV in Scheme F and is paired with the solvent flow rate downstream of the absorber (FC_1). This control scheme has shown promising performance with respect to system response [51].

Table 6 contains all the CV-MV pairs and the resulting tuning parameters for the control schemes studied with respect to operation with varying availability of steam for CO_2 capture.

Table 6: Tuning parameters for control schemes applied to operation with varying steam availability for CO_2 capture, including regulatory and higher-level controllers, as well as their respective set-points.

Scheme	CV	MV	K	τ [s]
E	L_1	FC_1	955	960
E	L_2	FC_3	358	960
E	L_3	FC_5	500	200

F	L_1	FC_2	918	960
F	L_2	FC_3	358	960
F	L_3	FC_5	500	200
F	T_{reb}	FC_1	157	60

CV, Control variable; MV, variable to manipulate; K, proportional gain; τ, time constant.

6 Results and discussion

6.1 Performance of the power plant model

The dynamic model is assessed for a selection of the key performance indicators under steady-state operational conditions in the load range of 100%–40% in Table 7. The design data in Table 7 refers to results from the simplified model of the reference plant operating with the fuel specifications presented in Table 1. The steady-state predictions of the dynamic model are within 2% of the design data for all the load conditions, except for the feed-water temperature at the boiler inlet, which is under-predicted by the dynamic model by a margin of 3%–11%. It should be noted that the generated power shows a perfect match owing to the controller set-point.

Table 7: Key performance indicators for steady-state operation at various loads derived from the simplified power plant model and from the dynamic model simulations.

Load	100%		80%		60%		40%	
	Dynamic model	Design data	Dynamic model	Design data	Dynamic model	Design data	Dynamic model	Design data
Live steam pressure [bar]	279.9	280	230.3	234	177.1	180.6	120.9	123.5
Live steam temperature [°C]	580	580	580	580	580	580	580	580
Reheat pressure [bar]	70.5	70	57.3	57.7	43.7	44.3	29.5	30.1
Reheat temperature [°C]	580	580	575.7	580	574.7	580	569.4	580
Feed-water temperature to boiler [°C]	248	256	238.1	248.2	225.3	237.9	207.4	233.5
Feed-water total mass flow [kg/s]	292.4	292.4	236.6	239.7	179.1	182.8	120.2	123.5
Fuel input [kg/s]	34	33.9	28	28.4	21.7	22.1	15	15.4
Generated power [MW]	408	408	334	334	256	256	173	173
Electric efficiency [%]	45.0	45.1	44.9	45.3	44.5	44.7	44.0	43.7

Data for the validation of supercritical PF power plant dynamics is scarce. Therefore, the response of the model in the present work is evaluated against the model used by Paranjape [30]. Paranjape developed a dynamic model of a supercritical coal-fired unit with advanced nonlinear control schemes and compared them with more traditional coordinated control loops. Paranjape [30] used a ramp rate of 5% per minute to ramp the power plant load between two load points. For the same load change as applied by Paranjape, a 95% settling time of 6–8 minutes is achieved for the power plant power output using our model, which is comparable to the settling time observed by Paranjape. Thus, a representative dynamic behavior can be expected for the power plant model.

6.2 Varying the power plant load

Figure 4 gives the simulated response of the power output and the fuel feed rate in the power plant without CO_2 absorption. The simulated responses of the selected performance indicators in the integrated system operating with different control schemes are presented in Figures 5 and 6, for Case 1 and Case 2, respectively. The calculated settling times for these performance indicators are shown in Tables 8 and 9. Figures 7 and 8 show the set-point deviations of the higher-level CVs of the CO_2-absorption process, as well as the set-point deviations of the power output, for Cases 1 and 2, respectively.

6.2.1 Comparison of power plants with and without CO_2 absorption

A comparison of the simulated responses to the same load profile of the power plant with and without CO_2 absorption are shown in Figures 4–6a for the generated power and in Figures 4b, 5e, and 6e for the fuel feed rate. The settling times with respect to generated power (6–9 minutes) are similar in the two systems. An exception to this is when Scheme B is applied in the integrated system, resulting in significantly longer settling times for both the power plant and the CO_2-absorption process. It is noteworthy that the settling times obtained for the CO_2-absorption process in the present work are comparable to those reported in previous studies of plants of comparable scale and residence times, see e.g. Lawal, et al. [13] and Flø, et al. [36]. For most of the parameters in Schemes A–D, the settling time is similar regardless of whether the power plant load is ramped up or down, though some difference is observed between ramping up and down, illustrating the non-linearity of the system. For Schemes A, C, and D, settling times of 1–1.5 hours are generally obtained for the performance indicators in the CO_2-absorption process presented in Table 9 when a 95% settling time is considered, and 1.5-4 hours when considering a 99% settling time.

The simulation results show that the interaction between the power plant and the CO_2-absorption process through the steam draw-off does not disrupt significantly the power plant operation and, consequently, does not strongly influence the power plant´s load-following capabilities. It should be noted that the steady-state value of the fuel flow in the integrated system and, consequently, the thermal input to the steam cycle, differs within 1.5% from the fuel flow in the power plant without CO_2 absorption.

A slightly faster settling time in the generated power is observed in the integrated system in Case 2, where the CO_2-capture rate is not an operating constraint, i.e., applying Scheme D. In this control scheme, the reboiler temperature is tightly controlled by regulating the valve position in the steam extraction line, and the solvent flow upstream of the absorber is kept constant, meaning that only one higher-level feed-back control loop is active in the CO_2-absorption process. Since the solvent flow is constant throughout the operation, a small change in the steam flow to the reboiler is required to maintain the set temperature, as shown in Figure 6c. On the power plant side, a larger share of the electricity production takes place in the high- and intermediate-pressure sections of the steam turbines in the integrated system, as compared with the power plant without CO_2 absorption, since around half of the steam mass flow that exits the IP turbine is directed to the reboiler. Consequently, the relative and absolute changes in mass flow through the LP section of the steam cycle are smaller in the integrated system. This results in a relatively smaller disturbance being induced in the LP section of the steam cycle in the integrated plant, which accounts for the slightly faster stabilization of the power output.

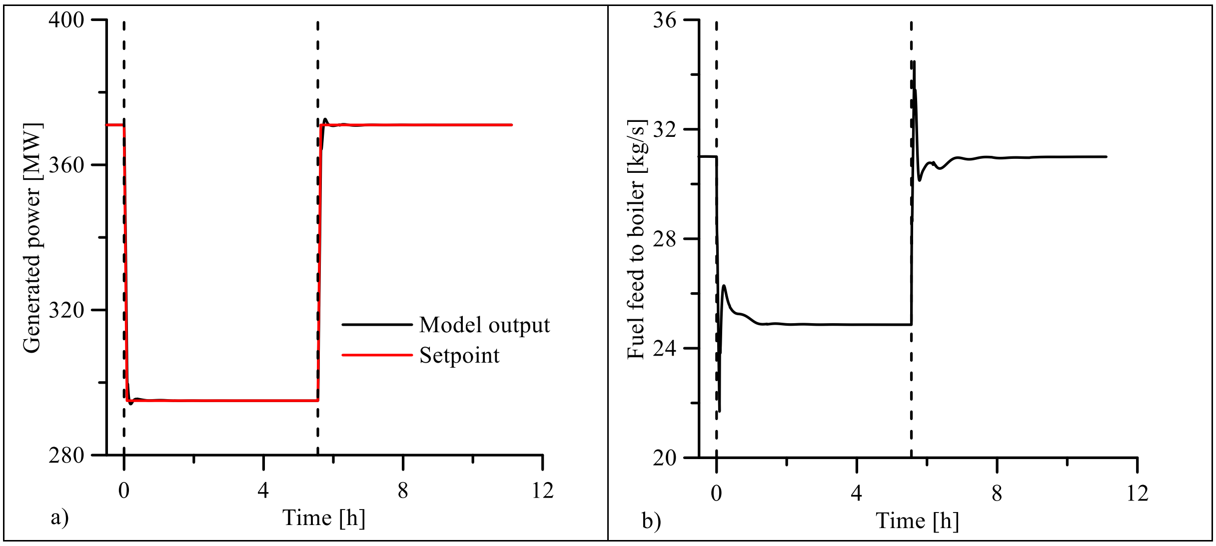

Figure 4: Responses of the a) power output and b) fuel feed to the boiler by a power plant without CO_2 absorption and with a load profile of 90%–70%–90%. The vertical dashed lines indicate the start of a load change.

Table 8: Settling times (95%) for the power output in power plant without CO_2 absorption.

	Settling time, 95% (min)		Settling time, 99% (min)	
Performance indicator	Ramp-down, 90% to 70%	Ramp-up, 70% to 90%	Ramp-down, 90% to 70%	Ramp-up, 70% to 90%
Generated power	6.7	7.9	12.8	15.7

6.2.2 Comparison of operational objectives for the CO_2-absorption process

Case 1, where maintaining the CO_2-capture rate is considered an operational objective, shows a slower response than Case 2, where the CO_2-capture rate is not a CV, in terms of deviation from the set-point of the generated power (*cf*. Figures 7 and 8). The power output stabilizes faster with Schemes C and D applied in Case 2 (see Figures 5a and 6a), as these schemes do not need to consider a feedback control loop of solvent recirculation in their CV-MV pairs. The solvent flow rate in both control schemes in Case 2 is relatively high, resulting in a CO_2-capture rate of >90% (*cf*. Figure 6d), as well as an increased steam requirement in the reboiler, relative to Case 1, which is to maintain the set temperature (Figures 5c and 6c). Consequently, the power plant electric efficiency is lower in Case 2 than in Case 1, which can be seen from Figures 5b and 6b. The increased energy requirement is especially pronounced for Scheme D (Figure 6f), where the solvent flow rate is highest, and this results in the highest fuel consumption within the power plant (Figures 5e and 6e). Due to the high CO_2 capture rate achieved in Case 2, the power plant specific CO_2 emissions are drastically decreased compared to Case 1 (Figures 5g and 6g).

In Case 1, Scheme A exhibits better dynamic performance than Scheme B. This is clearly illustrated by the transition rate of the reboiler steam flow to the new steady-state value (in Figure 5c), as well as by the deviation from the power output set-point during load change (in Figure 8). The CO_2-capture rate in Scheme B also adjusts slowly (*cf*. Figure 5d), due to the CO_2-capture rate being controlled by the steam flow rate to the reboiler, which results in a considerable time delay between the two variables. Consequently, the specific heat requirement also adjusts slowly and fluctuates in the same manner as the steam flow rate to the reboiler in Scheme B (*cf*. Figure 5f). Scheme A consists of two relatively fast high-level control loops, which result in not only more rapid responses, but also sharp overshoots of the manipulated variables during ramping, as observed for the reboiler steam flow and fuel feed flow in Figure 5, c and e, respectively.

Comparing the schemes for Case 2, Scheme C shows superior performance in terms of steady-state performance and settling times (*cf.* Figure 6 and Table 9). A time delay, i.e., the time from when a disturbance is introduced to the system until a response is observed, of 49 minutes is observed in the response of the reboiler temperature and, consequently, in the steam flow to the reboiler in Scheme D, as shown in Figure 6c, both when ramping up and ramping down. In Scheme D, the solvent flow rate is constant throughout the whole operation, resulting in a significant time delay being introduced by the absorber sump and the lean-rich heat exchanger before a change in the reboiler operating conditions is observed and the controller action is initiated.

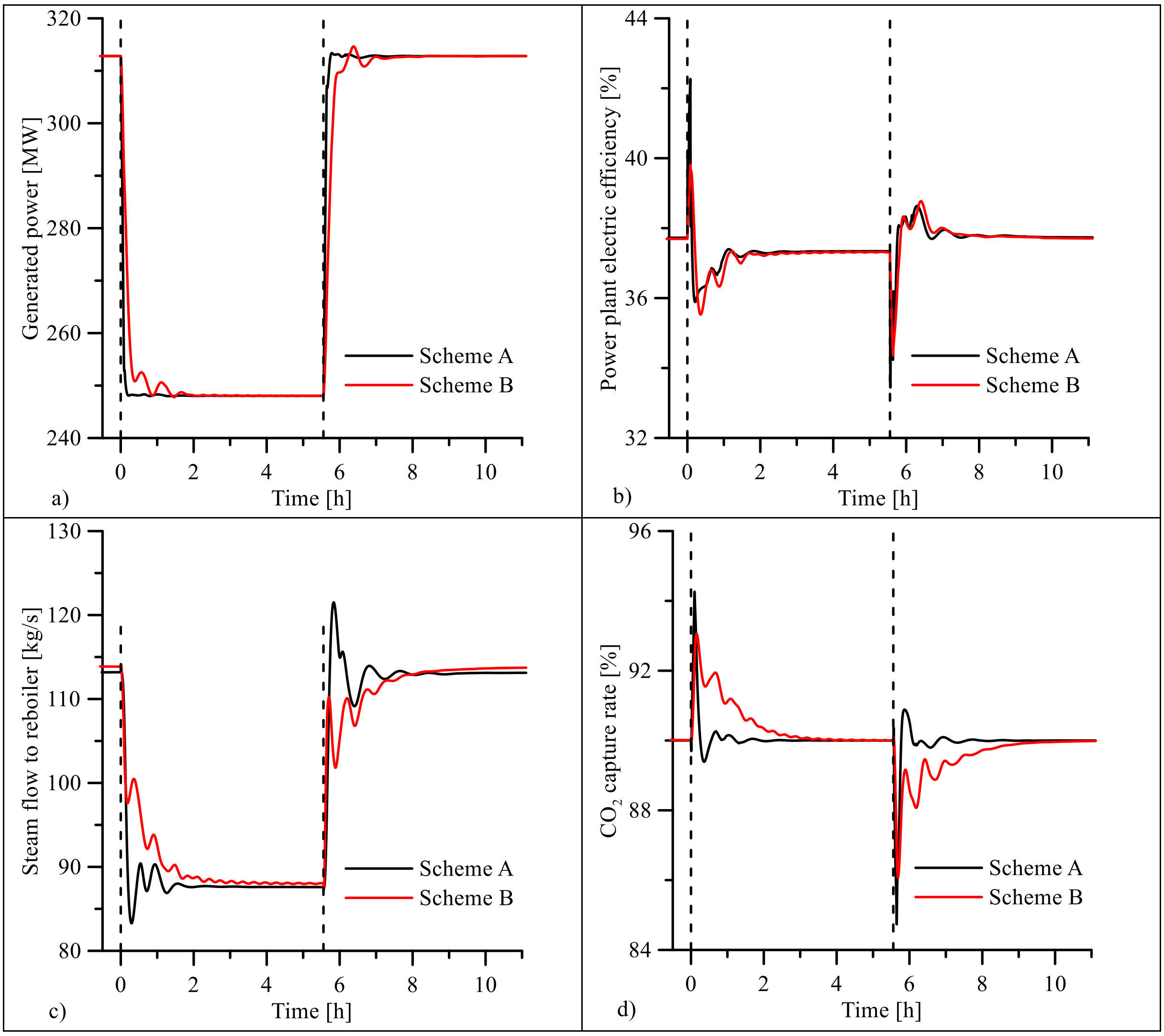

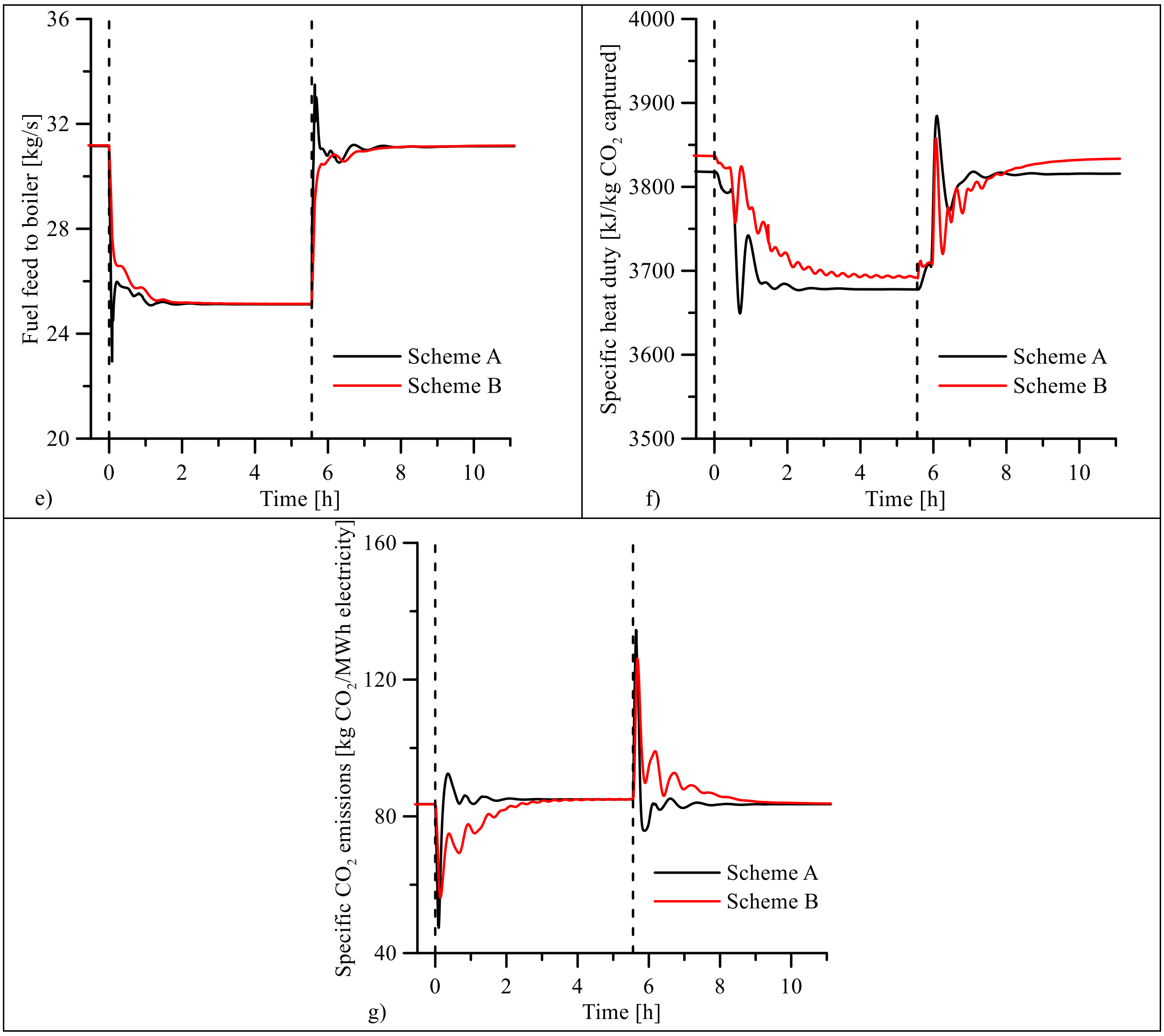

Figure 5: Responses in a power plant with CO_2 absorption for a load profile of 90%–70%–90% where the CO_2-capture rate is considered a constraint (Case 1). The vertical dashed lines indicate the start of a load change.

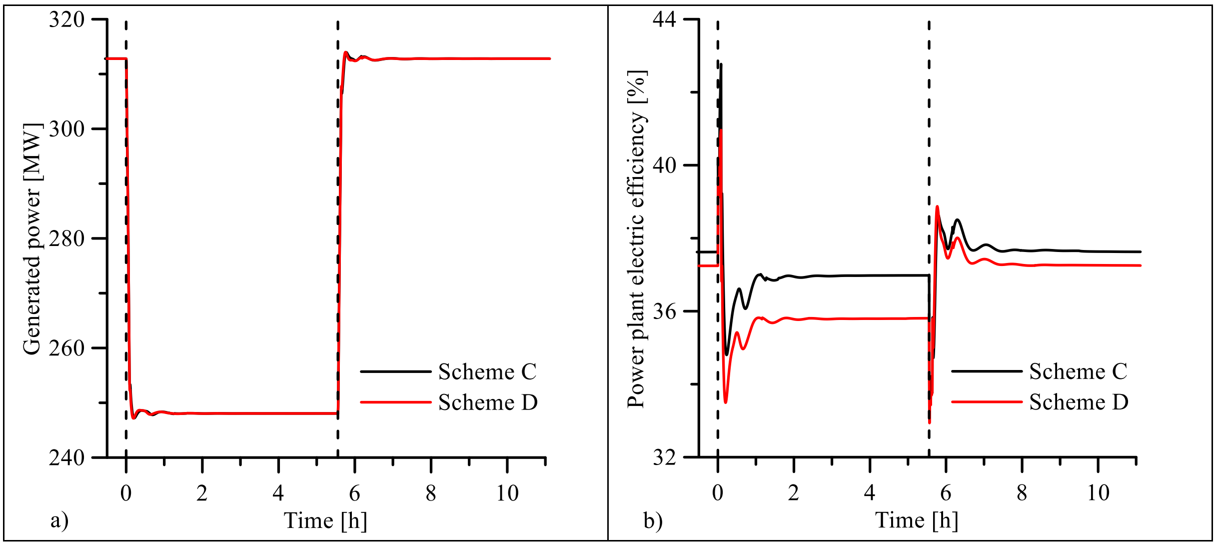

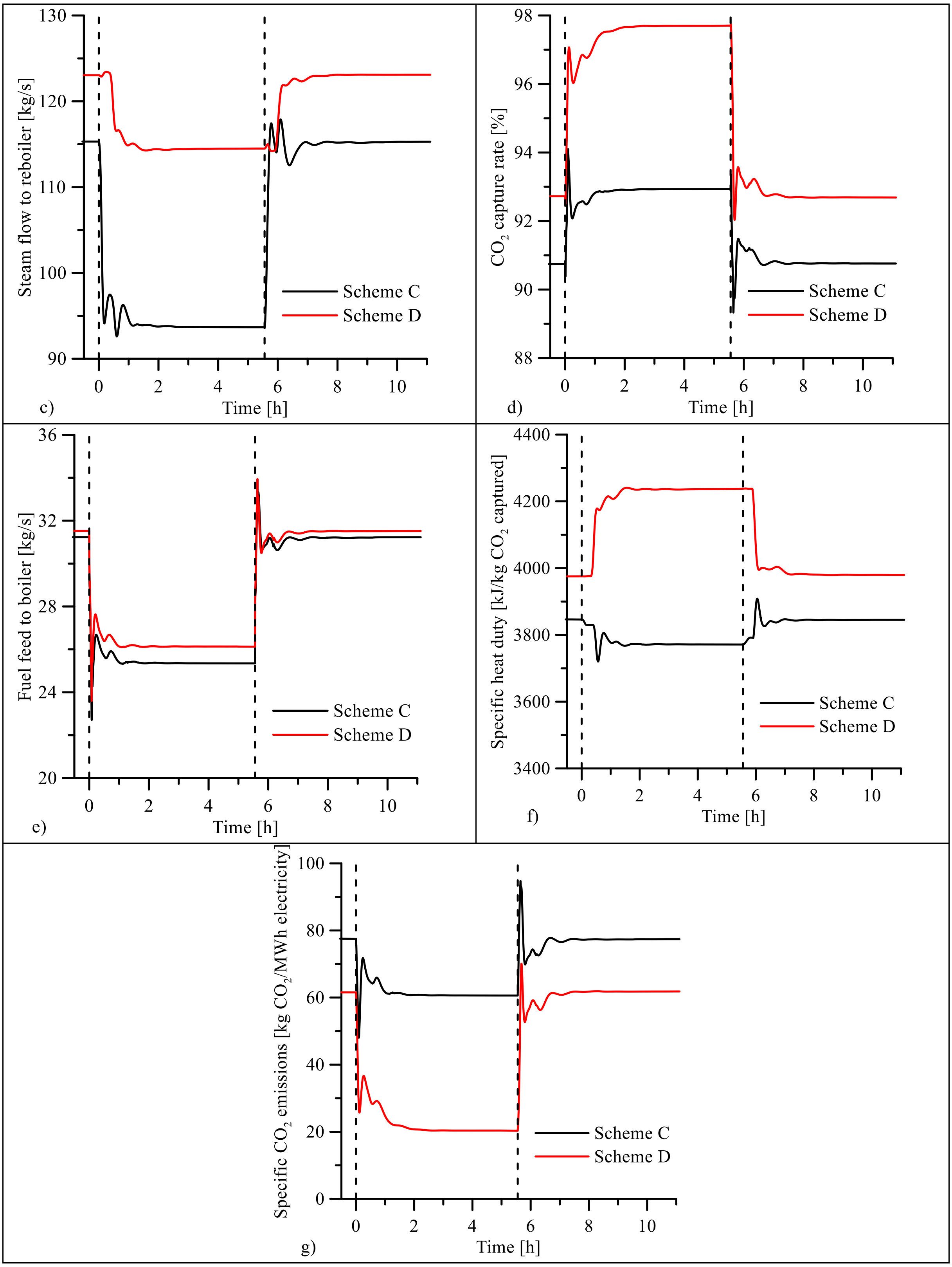

Figure 6: Responses in a power plant with CO_2 absorption for a load profile of 90%–70%–90% where the CO_2 capture rate is not considered a constraint (Case 2). The vertical dashed lines indicate the start of a load change.

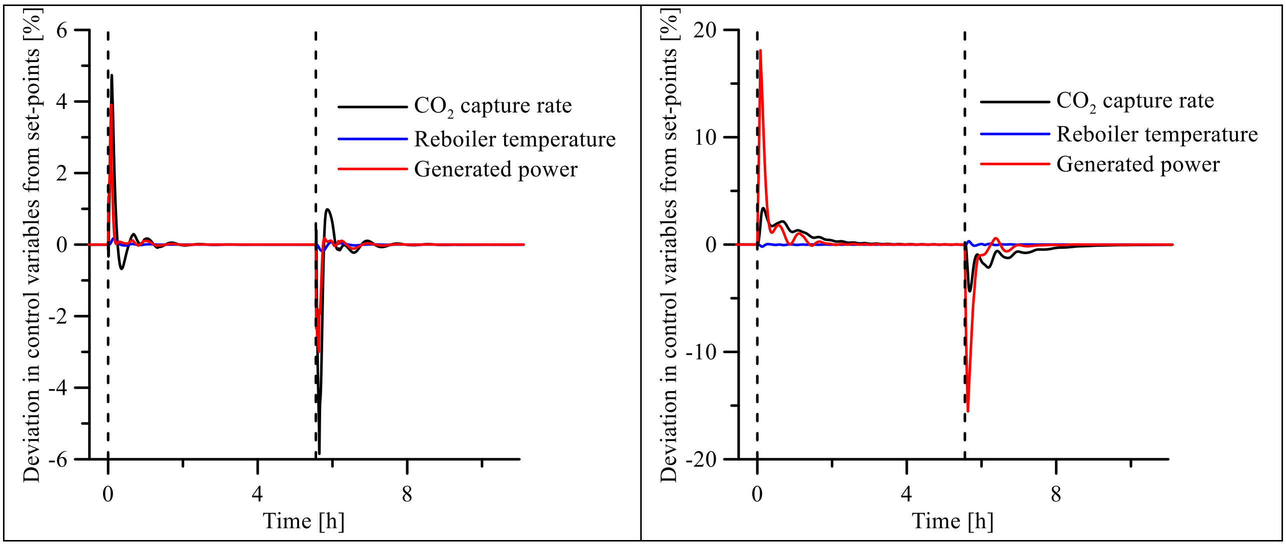

Figure 7: Deviation from their set-points of the higher-level CVs for the CO_2-absorption process and the power plant output for Case 1, Scheme A (left panel) and Scheme B (right panel). Note the difference in scale of the *y*-axes. The vertical dashed lines indicate the start of a load change.

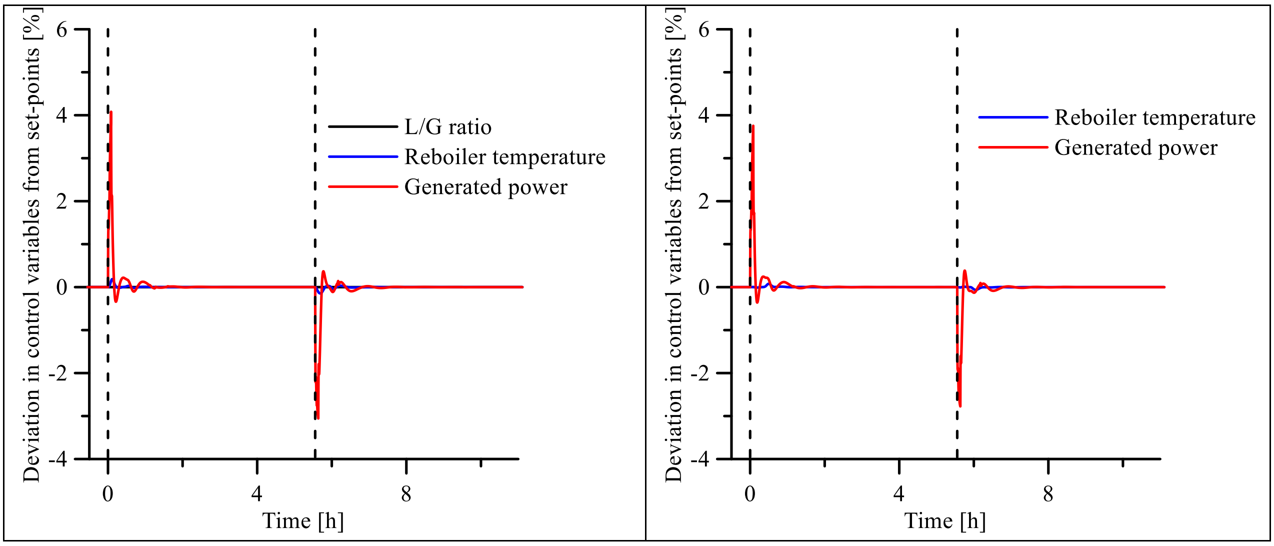

Figure 8: Deviations from their set-points of the higher-level CVs for the CO_2-absorption process and the power plant output for Case 2, Scheme C (left panel) and Scheme D (right panel). The vertical dashed lines indicate the start of a load change.

Table 9: Settling times for selected performance indicators from the simulations in which power plant load is varied. The settling time for the CO_2-capture rate is not shown for Case 1 (Schemes A and B), as it is a control variable in this case, and the settling time for the solvent circulation rate is not shown for Scheme D, as it is kept constant.

		Settling time, 95% (min)		Settling time, 99% (min)	
Performance indicator	Case – scheme	Ramp-down, 90% to 70%	Ramp-up, 70% to 90%	Ramp-down, 90% to 70%	Ramp-up, 70% to 90%
Generated power	1 – A	7.3	8.9	9.9	10.8
	1 – B	40.8	23.5	100.9	78.7
	2 – C	7.4	8.5	14.6	16.3
	2 – D	6.9	7.7	13.0	14.5
Steam flow to reboiler	1 – A	64.2	62.2	100.7	153.6
	1 – B	95.1	122.9	184.4	214.5
	2 – C	59.0	64.5	105.5	110.7
	2 – D	74.5	87.7	151.7	130.8

CO_2 capture rate	1 – A	-	-	-	-
	1 – B	-	-	-	-
	2 – C	60.0	54.9	106.2	102.0
	2 – D	72.4	59.2	131.6	102.6
Solvent circulation rate	1 – A	57.5	57.9	100.7	106.1
	1 – B	113.3	136.4	202.9	234.1
	2 – C	55.0	57.8	97.0	105.5
	2 – D	-	-	-	-

6.3 Varying the steam availability for CO_2 capture

The simulated responses of performance indicators in the integrated system during a period of reduced steam flow to the CO_2-absorption process is shown in Figure 9. For Schemes E and F, the system does not reach a steady state during the 2 hours of a hypothetical peak-load demand, and the generated power fluctuates by ±4 MW from the target value of 360 MW, although it approaches stable generation. The calculated settling times for the performance indicators are shown in Table 10. Table 10 shows only the settling times for the transition from reduced steam availability for CO_2 capture to normal operation at full load, since the integrated system did not reach a new steady state within the 2 hours when operating with increased power output due to the aggressive disturbance introduced to the system and the lack of tight flow control in the stream extraction line in this mode of operation.

In Scheme E, rapid responses are observed in the power plant. However, sharp overshoots in the generated power, the steam flow to reboiler, and the steam flow through the final stage of the LP turbine are observed when the steam valve position is changed to reduce the steam flow to the CO_2-absorption process (*cf.* Figure 9, a, b, c and e). In Scheme E, a time delay of 51 minutes is observed in the response of the CO_2-capture rate, as shown in Figure 9d. Here, the L/G ratio is kept constant, which essentially means that the solvent flow is constant, as no changes are induced in the combustion process of the power plant, and consequently, there are no changes in the flue gas flow, during the operation. As the steam flow to the reboiler decreases rapidly, a rapid drop in reboiler temperature is observed in Figure 9f, resulting in an increase in the specific heat duty in the reboiler (*cf.* Figure 9g). The time delay introduced by the stripper sump, solvent heat exchanger, and buffer tank means that the increase in lean loading in the absorber inlet is delayed, which explains the time delay observed for the CO_2-capture rate response, and consequently in the power plant´s specific CO_2 emissions (*cf.* Figure 9h).

In Scheme F, rapid responses are observed in both the power plant and the CO_2-absorption process, although these responses are considerably smoother that those seen in Scheme E, in terms of the overshoots of the steam flows and generated power (*cf.* Figure 9, a, b, c and e). Furthermore, significantly shorter settling times are observed in Scheme F than in Scheme E, as shown in Table 10. The reboiler temperature is relatively tightly controlled by the solvent circulation rate, and a deviation of only ±1°C from the temperature set-point is observed in Figure 9f, when the steam extraction valve position is changed. In contrast, considerable fluctuations are observed in the CO_2-capture rate, as shown in Figure 9d. As the solvent flow rate downstream of the absorber is adjusted to maintain the reboiler temperature, the solvent flow rate upstream of the absorber is adjusted to maintain a set liquid level in the absorber sump, with consequent effect on the CO_2-capture rate.

The operation with varying steam availability for CO_2 capture is considered in the framework of a day-ahead energy market, where electricity is sold by the hour. The observed fluctuations should therefore not prevent the power plant from participating in the market, where the plant operator receives revenues for the electricity produced within the hour.

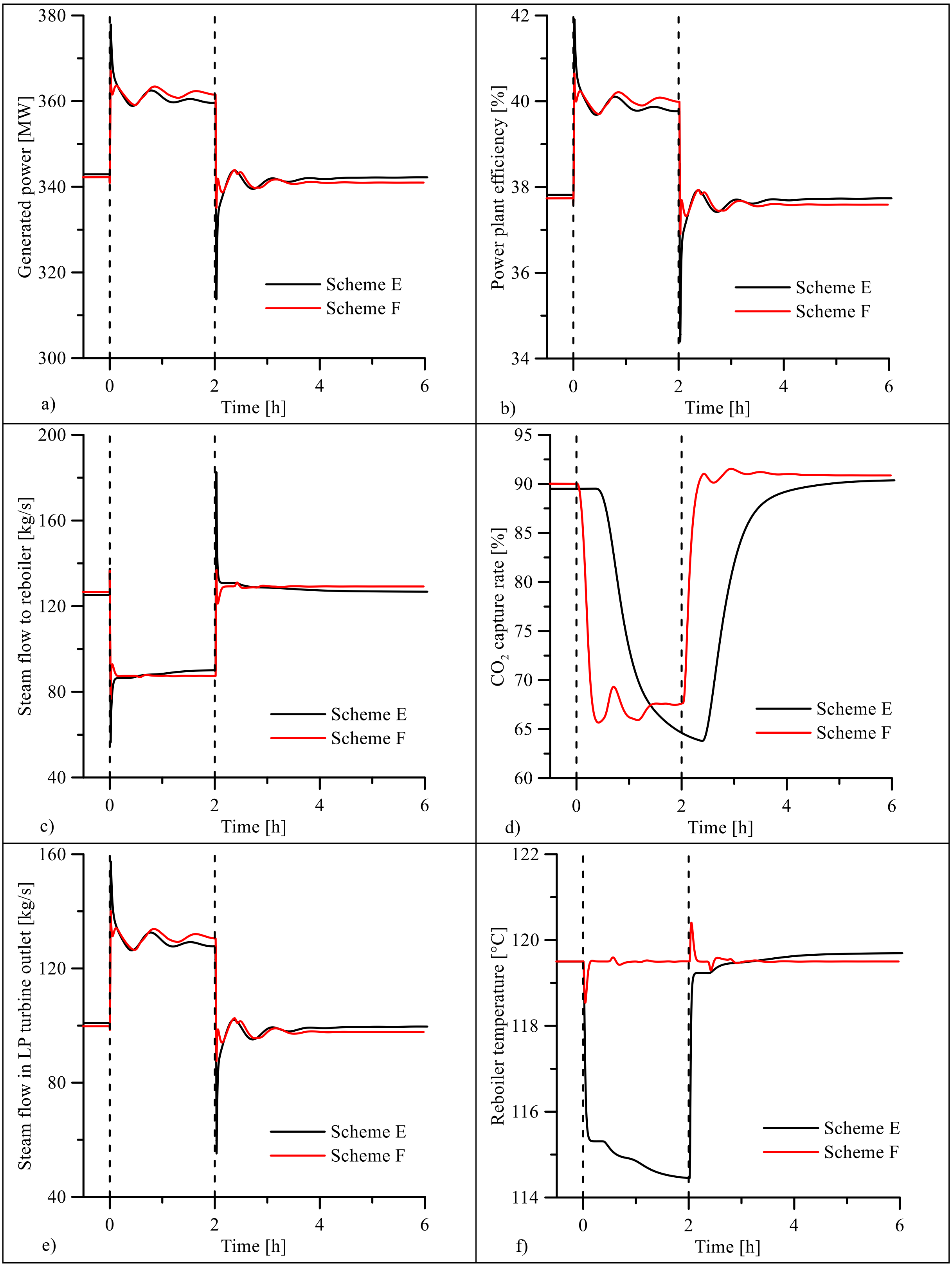

a)
Generated power [MW]
Time [h]
Scheme E
Scheme F
b)
Power plant efficiency [%]
Time [h]
Scheme E
Scheme F
c)
Steam flow to reboiler [kg/s]
Time [h]
Scheme E
Scheme F
d)
CO_2 capture rate [%]
Time [h]
Scheme E
Scheme F
e)
Steam flow in LP turbine outlet [kg/s]
Time [h]
Scheme E
Scheme F
f)
Reboiler temperature [°C]
Time [h]
Scheme E
Scheme F

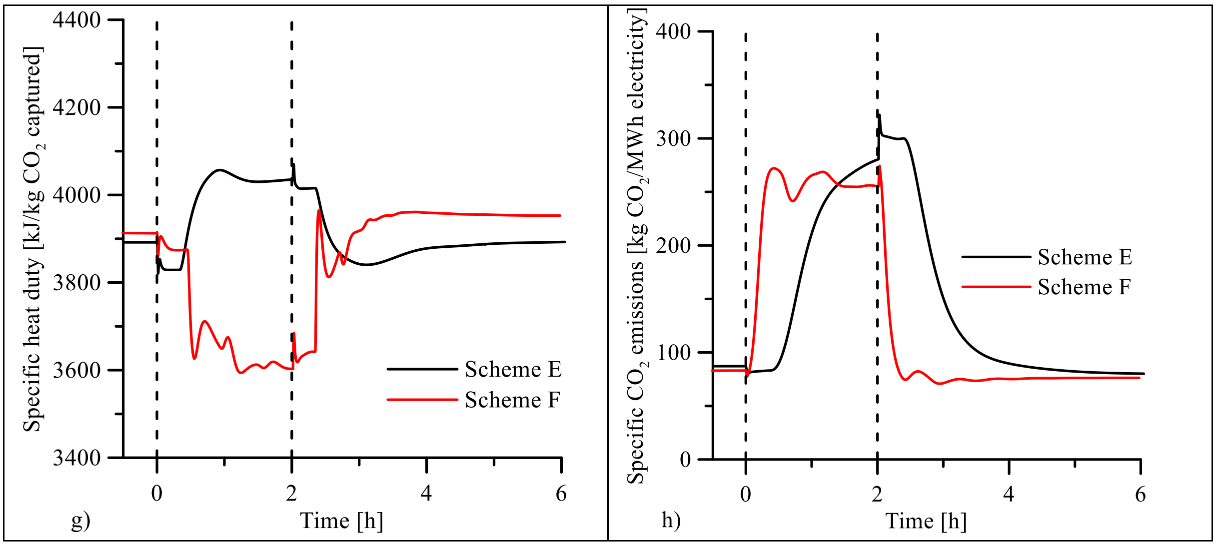

Figure 9: Effects of decreasing the amount of steam available for CO_2 capture so as to increase the power output in response to the peak-load demand, by applying a ramp (at t=0) for 1 minute to the valve position in the steam extraction line leading to the CO_2-absorption process. This condition is sustained for 2 hours before operation is returned to full load (100%), with no restrictions placed on steam availability. The vertical dashed lines indicate the start of a change in the load.

Table 10: Settling times for selected performance indicators from the simulations in which the availability of steam for CO_2 capture was varied. Only the settling times for the transition from reduced steam availability for CO_2 capture to normal operation at full load are shown. No settling time is listed for the solvent circulation rate in Scheme E, given that it is constant, and no settling time is listed for the reboiler temperature in Scheme F, as it is a control variable in this scheme.

Performance indicator	Scheme	Settling time, 95% (min)	Settling time, 99% (min)
Generated power	E	90.4	145.4
	F	53.4	95.7
CO_2 capture rate	E	116.3	193.1
	F	17.3	95.7
Reboiler temperature	E	41.8	139.1
	F	-	-
Solvent circulation rate	E	-	-
	F	41.4	121.9

7 Conclusions

In this work, a dynamic model of a supercritical PF coal-fired plant retrofitted with an MEA-based CO_2-absorption process was developed. Previous studies that have focused on the controllability of CO_2-absorption processes have generally disregarded the dynamic interactions that occur between the CO_2-absorption process and the power plant. The novelty of the current work lies in the linking of the two detailed dynamic process models and evaluating control schemes for the CO_2-absorption process within the integrated system, with the focus on stable operation of the power plant. Two modes of power plant operation are considered: varying the power plant load; and varying the steam availability for CO_2 capture.

For operation of the power plant with varying load, two cases with different operational objectives for the CO_2-absorption process are considered in which: 1) the CO_2-capture rate is an operational constraint; and 2) the CO_2 capture rate is not a constraint. Furthermore, operation of the power plant with varying load with and without CO_2-absorption is investigated. The results of the simulations show that the power output stabilizes within a similar time-frame for the two systems, albeit a few minutes faster for the power plant without CO_2 absorption. Thus, the CO_2-absorption process does not affect significantly the power plant´s load-following capabilities. When operating with varying power plant load, the settling times observed for the CO_2-absorption process are on average 1–2 hours, i.e., considerably longer than the settling times for the power output, which are on average 6–9 minutes. It is relatively efficient to control the CO_2 capture rate to an operational requirement by controlling the lean solvent flow rate (Scheme A). A more stable power generation is achieved when the CO_2 capture rate is not considered to be an operational constraint, in this case the L/G ratio control (Scheme C) results in higher part-load efficiency of the power plant. However, the decrease in power plant efficiency with the power plant load is higher when the CO_2 capture rate is allowed to fluctuate, due to the relatively high rate of solvent circulation and consequent high flow rate of steam extracted to maintain the reboiler temperature at its set-point.

When operating with varying steam availability for CO_2 capture, the steam flow is defined by the power plant, and the CO_2 capture rate is disregarded as an operational constraint. During the two hours of reduced availability of steam for CO_2 capture, the integrated system does not stabilize with either of the investigated control schemes, although it approaches steady-state during the operation. The reboiler temperature is better controlled by the solvent flow rate (Scheme F) rather than the L/G ratio (Scheme E), resulting in less-prominent overshoots in steam flow and generated power, as well as shorter settling times. Future research should investigate how this type of operation could be improved, possibly with more advanced control systems, and how the integrated system responds to providing ancillary services to the power grid on even shorter timescales.

Supporting information

Off-design heat transfer coefficient exponent, tuning parameters for power plant control loops, schematic overview of dynamic PF power plant model including controllers and measurement points

Acknowledgments

This work has been financially supported by the Chalmers Energy Initiative, the Landsvirkjun Energy Research Fund, and the Swedish Energy Agency. The authors also acknowledge the Department of Energy and Process Engineering at the Norwegian University of Science and Technology (NTNU), for funding parts of this project.

References

1. European Commission. 2030 framework for climate and energy policies. http://ec.europa.eu/clima/policies/2030/index_en.htm.
2. Morthost, P. E.; Ray, S.; Munksgaard, J.; Sinner, A.-F. *Wind Energy and Electricity Prices - Exploring the 'merit order effect'*; European Wind Energy Association: 2010.
3. Wang, M.; Lawal, A.; Stephenson, P.; Sidders, J.; Ramshaw, C., Post-combustion CO_2 capture with chemical absorption: A state-of-the-art review. *Chem. Eng. Res. Des.* **2011,** *89* (9), 1609-1624.
4. Stéphenne, K. In *Start-up of world's first commercial post-combustion coal fired ccs project: Contribution of shell cansolv to saskpower boundary dam iccs project*, Energy Procedia, 2014; pp 6106-6110.
5. Bui, M.; Gunawan, I.; Verheyen, V.; Feron, P.; Meuleman, E.; Adeloju, S., Dynamic modelling and optimisation of flexible operation in post-combustion CO2 capture plants—A review. *Comput. Chem. Eng* **2014,** *61* (0), 245-265.
6. Ziaii, S. Dynamic Modeling, Optimization, and Control of Monoethanolamine Scrubbing for CO_2 Capture. The University of Texas at Austin, 2012.

7. Cormos, A.-M.; Vasile, M.; Cristea, M.-V., Flexible operation of CO_2 capture processes integrated with power plant using advanced control techniques. *Comput.-Aided Chem. Eng.* **2015,** *37*, 1547-1552.
8. Panahi, M.; Skogestad, S., Economically efficient operation of CO2 capturing process part I: Self-optimizing procedure for selecting the best controlled variables. *Chem. Eng. Process.* **2011,** *50* (3), 247-253.
9. Panahi, M.; Skogestad, S., Economically efficient operation of CO2 capturing process. Part II. Design of control layer. *Chem. Eng. Process.* **2012,** *52*, 112-124.
10. Gaspar, J.; Ricardez-Sandoval, L.; Jørgensen, J. B.; Fosbøl, P. L., Controllability and flexibility analysis of CO2 post-combustion capture using piperazine and MEA. *International Journal of Greenhouse Gas Control* **2016,** *51*, 276-289.
11. Nittaya, T.; Douglas, P. L.; Croiset, E.; Ricardez-Sandoval, L. A., Dynamic modelling and control of MEA absorption processes for CO2 capture from power plants. *Fuel* **2014,** *116*, 672-691.
12. Walters, M. S.; Edgar, T. F.; Rochelle, G. T., Regulatory Control of Amine Scrubbing for CO2 Capture from Power Plants. *Ind. Eng. Chem. Res.* **2016,** *55* (16), 4646-4657.
13. Lawal, A.; Wang, M.; Stephenson, P.; Obi, O., Demonstrating full-scale post-combustion CO_2 capture for coal-fired power plants through dynamic modelling and simulation. *Fuel* **2012,** *101*, 115-128.
14. Wellner, K.; Marx-Schubach, T.; Schmitz, G., Dynamic Behavior of Coal-Fired Power Plants with Postcombustion CO_2 Capture. *Ind. Eng. Chem. Res.* **2016,** *55*, 12038-12045.
15. Mac Dowell, N.; Shah, N., Dynamic modelling and analysis of a coal-fired power plant integrated with a novel split-flow configuration post-combustion CO_2 capture process. *Int. J. Greenhouse Gas Control* **2014,** *27* (0), 103-119.
16. Mac Dowell, N.; Shah, N., The multi-period optimisation of an amine-based CO2 capture process integrated with a super-critical coal-fired power station for flexible operation. *Comput. Chem. Eng* **2015,** *74*, 169-183.
17. Hanak, D. P.; Biliyok, C.; Manovic, V., Evaluation and modeling of part-load performance of coal-fired power plant with postcombustion CO<inf>2</inf> capture. *Energy Fuels* **2015,** *29* (6), 3833-3844.
18. Garðarsdóttir, S. Ó.; Normann, F.; Andersson, K.; Prölß, K.; Emilsdóttir, S.; Johnsson, F., Post-combustion CO_2 capture applied to a state-of-the-art coal-fired power plant - The influence of dynamic process conditions. *Int. J. Greenhouse Gas Control* **2015,** *33*, 51-62.
19. Montañés, R. M.; Korpås, M.; Nord, L. O.; Jaehnert, S., Identifying operational requirements for flexible CCS power plant in future energy systems. *Energy Procedia* **2016,** *86*, 22-31.
20. Modelica and the Modelica Association. https://modelica.org/.
21. Hardarson, B.; Storm, J. Heat Integration of Chilled Ammonia Process in a Pulverized Coal Power Plant. Chalmers University of Technology, Gothenburg, Sweden, 2008.
22. Modelon. Thermal Power Library. http://www.modelon.com/products/modelica-libraries/thermal-power-library/.
23. Modelon. Post-Combustion Capture with Amine Solutions. http://www.modelon.com/fileadmin/user_upload/Industries/Energy_Process/CCS/PostCombustionCapture_flyer.pdf.
24. Rovira, A.; Valdés, M.; Durán, M. D., A model to predict the behaviour at part load operation of once-through heat recovery steam generators working with water at supercritical pressure. *Appl. Therm. Eng.* **2010,** *30* (13), 1652-1658.
25. Nord, L. O.; Anantharaman, R.; Bolland, O., Design and off-design analyses of a pre-combustion CO2 capture process in a natural gas combined cycle power plant. *Int. J. Greenhouse Gas Control* **2009,** *3* (4), 385-392.
26. Nord, L. O. Pre-combustion CO_2 capture: Analysis of integrated reforming combined cycle. Doctoral Thesis, Norwegian University of Science and Technology, Trondheim, Norway, 2010.
27. Cooke, D. H., On Prediction of Off-Design Multistage Turbine Pressures by Stodola´s Ellipse. *J. Eng. Gas Turbines Power* **1985,** *107* (3), 596-606.
28. Beebe, R., Condition monitoring of steam turbines by performance analysis. *Journal of Quality in Maintenance Engineering* **2003,** *9* (2), 102-112.
29. Bolland, O., Thermal power generation. Department of Energy and Process Engineering, Norwegian University of Science and Technology: 2014.
30. Paranjape, R. D. Modeling and control of a supercritical coal fired boiler. PhD. Thesis, Texas Tech University, 1996.
31. Thulukkanam, K., *Heat Exchanger Design Handbook*. 2nd Edition ed.; CRC Press: 2013.
32. Numrich, R.; Müller, J., J1 Filmwise Condensation of Pure Vapors. In *VDI Heat Atlas*, Springer Berlin Heidelberg: 2010; pp 903-918.
33. Gnielinski, V., G1 Heat Transfer in Pipe Flows. In *VDI Heat Atlas*, 2nd edition ed.; Springer Berlin Heidelberg: 2010; pp 691-700.

34. ENTSO-E *ENTSO-E at a Glance*; European Network of Transmission System Operators for Electricity: 2015.
35. Aske, E. M. B.; Skogestad, S., Consistent Inventory Control. *Ind. Eng. Chem. Res.* **2009,** *48*, 10892-10902.
36. Flø, N. E.; Kvamsdal, H. M.; Hillestad, M.; Mejdell, T., Dominating dynamics of the post-combustion CO2 absorption process. *Comput. Chem. Eng* **2016,** *86*, 171-183.
37. Flø, N. E.; Knuutila, H.; Kvamsdal, H. M.; Hillestad, M., Dynamic model validation of the post-combustion CO_2 absorption process. *Int. J. Greenhouse Gas Control* **2015,** *41*, 127-141.
38. Garðarsdottir, S. Ó.; Normann, F.; Andersson, K.; Johnsson, F., Post-combustion CO_2 capture using monoethanolamine and ammonia solvents: The influence of the CO_2 concentration on the technical performance. *Ind. Eng. Chem. Res.* **2015,** *54* (2), 681-690.
39. Bravo, J. L.; Rocha, J. A.; Fair, J. R., A comprehensive model for the performance of columns containing structured packings. *Inst. Chem. Eng. Symp. Ser.* **1992,** *129* (A439).
40. Åkesson, J.; Laird, C. D.; Lavedan, G.; Prölß, K.; Tummescheit, H.; Velut, S.; Zhu, Y., Nonlinear Model Predictive Control of a CO_2 Post-Combustion Absorption Unit. *Chem. Eng. Technol.* **2012,** *35* (3), 445-454.
41. Montañés, R. M.; Dutta, R.; Nord, L. O.; Bolland, O.; Enaasen Flø, N., Dynamic process model development, parameter estimation and validation with transient plant data collected from a MEA test campaign at the CO2 Technology Transfer Center Mongstad. *Energy Procedia - In press* **2016**.
42. Peng, J.; Edgar, T. F.; Eldridge, R. B., Dynamic rate-based and equilibrium models for a packed reactive distillation column. *Chemical Engineering Science* **2003,** *58* (12), 2671-2680.
43. Razi, N.; Svendsen, H. F.; Bolland, O., Assessment of mass transfer correlations in rate-based modeling of a large-scale CO_2 capture with MEA. *Int. J. Greenhouse Gas Control* **2014,** *26*, 93-108.
44. Sanchez Fernandez, E.; Sanchez del Rio, M.; Chalmers, H.; Khakharia, P.; Goetheer, E. L. V.; Gibbins, J.; Lucquiaud, M., Operational flexibility options in power plants with integrated post-combustion capture. *International Journal of Greenhouse Gas Control* **2016,** *48, Part 2*, 275-289.
45. Liebenthal, U.; Pinto, D. D. D.; Monteiro, J. G. M. S.; Svendsen, H. F.; Kather, A., Overall Process Analysis and Optimisation for CO2 Capture from Coal Fired Power Plants based on Phase Change Solvents Forming Two Liquid Phases. *Energy Procedia* **2013,** *37*, 1844-1854.
46. Lucquiaud, M.; Gibbins, J., Retrofitting CO_2 capture ready fossil fuel plants with post-combustion capture. Part 1: requirements for supercritical pulverized coal plants using solvent-based flue gas scrubbing. *Proc. Inst. Mech. Eng., Part A* **2009,** *223* (3), 213-226.
47. Skogestad, S., Simple analytic rules for model reduction and PID controller tuning. *J. Process Control* **2003,** *13* (4), 291-309.
48. Henderson, C. *Increasing the flexibility of coal-fired power plants*; IEA Clean Coal Centre: 2014.
49. Jordal, K.; Ystad, P. A. M.; Anantharaman, R.; Chikukwa, A.; Bolland, O., Design-point and part-load considerations for natural gas combined cycle plants with post combustion capture. *Int. J. Greenhouse Gas Control* **2012,** *11*, 271-282.
50. Chalmers, H.; Lucquiaud, M.; Gibbins, J.; Leach, M., Flexible Operation of Coal Fired Power Plants with Postcombustion Capture of Carbon Dioxide. *J. Environ. Eng.* **2009,** *135*, 449-458.
51. Ziaii, S.; Rochelle, G. T.; Edgar, T. F., Dynamic Modeling to Minimize Energy Use for CO_2 Capture in Power Plants by Aqueous Monoethanolamine. *Ind. Eng. Chem. Res.* **2009,** *48*, 6105-6111.

Nomenclature and abbreviations

Cp	Heat capacity (J/kgK)
CV	Control variable
DCC	Direct contact cooler
DoF	Degree of freedom
E	Energy (J)
EOR	Enhanced oil recovery
FC	Flow controller
FGD	Flue gas desulfurization
FWH	Feed-water heating
h	Enthalpy
HHV	Higher heating value (MJ/kg)

HP	High pressure
IP	Intermediate pressure
K	Gain
L	Level
L/G	Liquid-to-gas
LHV	Lower heating value (MJ/kg)
LP	Low pressure
m	Mass (kg)
$\dot{m}$	Mass flow (kg/s)
MEA	Monoethanolamine
MPC	Model predictive control
MV	Manipulated variable
n	Exponent
p	Pressure (Pa)
P	Power (W)
PF	Pulverized fuel
PZ	Piperazine
Q	Heat (W)
RH	Reheater
SH	Superheater
t	Time (s)
T	Temperature (K)
U	Heat transfer coefficient, gas side (W/m^2K)
VRE	Variable renewable electricity
V	Volume (m^3)
WW	Water walls
x	Mass fraction

Greek symbols

ρ	Density (kg/m^3)
α	Heat transfer coefficient, water side (W/m^2K)
τ	Time constant (s)
η_{CO2}	CO_2-capture rate (%)
η_{el}	Power plant electric efficiency